THE JOURNAL OF BIOLOGICAL CHEMISTRY VOL. 286, NO. 36, pp. 31565–31575, September 9, 2011

Molecular Determinants within N Terminus of Orai3 Protein That Control Channel Activation and Gating*[S]

Received for publication, February 2, 2011, and in revised form, June 30, 2011 Published, JBC Papers in Press, July 1, 2011, DOI 10.1074/jbc.M111.227546

Judith Bergsmann[‡1], Isabella Derler[‡1,2], Martin Muik[‡], Irene Frischauf[‡3], Marc Fahrner[‡], Philipp Pollheimer[‡], Clemens Schwarzinger[§], Hermann J. Gruber[‡], Klaus Groschner[¶], and Christoph Romanin[‡4]

From the Institutes of [‡]Biophysics and [§]Chemical Technology of Organic Materials, University of Linz, Altenbergerstrasse 69, 4040 Linz, Austria and [¶]Department of Pharmaceutical Sciences-Pharmacology and Toxicology, University of Graz, Universitätsplatz 2, 8010 Graz, Austria

STIM1 and Orai represent the key components of Ca^{2+} release-activated Ca^{2+} channels. Activation of Orai channels requires coupling of the C terminus of STIM1 to the N and C termini of Orai. Although the latter appears to be central in the interaction with STIM1, the role of the N terminus and particularly of the conserved region close to the first transmembrane sequence is less well understood. Here, we investigated in detail the functional role of this conserved region in Orai3 by stepwise deletions. Molecular determinants were mapped for the two modes of Orai3 activation via STIM1 or 2-aminoethoxydiphenyl borate (2-APB) and for current gating characteristics. Increasing N-terminal truncations revealed a progressive decrease of the specific fast inactivation of Orai3 concomitant with diminished binding to calmodulin. STIM1-dependent activation of Orai3 was maintained as long as the second half of this conserved N-terminal domain was present. Further truncations abolished it, whereas Orai3 stimulation via 2-APB was partially retained. In aggregate, the N-terminal conserved region plays a multifaceted role in Orai3 current gating with distinct structural requirements for STIM1- and 2-APB-stimulated activation.

Ca^{2+} is a multifunctional messenger that regulates a variety of processes like muscle contraction, gene expression, proliferation, cell growth, and cell death. A major route for Ca^{2+} entry across the cell membrane is represented by the Ca^{2+} release-activated Ca^{2+} (CRAC)[5] channel (1–4). STIM1 and Orai proteins have been identified as the key components of the CRAC signaling machinery. STIM1, which is located in the endoplasmic reticulum membrane, acts as a Ca^{2+} sensor and as a transducer that triggers CRAC channel activation (5–7). Upon depletion of endoplasmic reticulum Ca^{2+} stores, STIM1 multimerizes and redistributes into punctae in close proximity to the plasma membrane (6, 8, 9). Here it co-localizes with the CRAC channel component Orai, culminating in channel activation followed by Ca^{2+} influx (7, 8, 10).

The Orai family comprises three members (Orai1–3), all of which form highly Ca^{2+}-selective channels upon coexpression with STIM1; however, they differ in fast Ca^{2+}-dependent inactivation and in their responses to 2-APB (3, 11–14). Fast inactivation of CRAC channels is mediated by the cooperative interplay of several structures within Orai proteins, the CRAC modulatory domain of STIM1, and via calmodulin (CaM) binding to the Orai N terminus (3, 11, 14–19). Low concentrations of 2-APB ($<10\ \mu$M) enhance store-operated Orai1 currents (20) together with an increased open probability (18). High 2-APB concentrations ($\geq 50\ \mu$M) completely or partially inhibit STIM1-mediated Orai1 or Orai2 currents, respectively (12, 21), whereas Orai3 is robustly stimulated by 2-APB independently of STIM1 and Ca^{2+} store depletion (12, 21–23). In addition, 2-APB alters the ion selectivity of Orai3 channels by increasing their pore size from ~3.8 Å to more than 5.34 Å (22). Lee *et al.* (11) have additionally demonstrated that an Orai3 chimera containing an Orai1 C terminus could be similarly activated by 2-APB like wild-type Orai3.

Store-dependent coupling of STIM1 and Orai is predominantly mediated by interaction of their C termini (10, 24) and involves a conformational transition within the STIM1 C terminus (25, 26). Although the role of the Orai C terminus in this coupling process has been extensively studied, much less is known about the function of the Orai N terminus. So far it has been hypothesized that a fully conserved N-terminal Orai region (*e.g.* aa 73–90 in Orai1 and aa 48–65 in Orai3) is essential for STIM1-dependent stimulation (19, 27–31). It has been reported recently that a single lysine within this conserved region (K85E in Orai1 and K60E in Orai3) represents a critipcal residue for store-operated activation (31). This conserved region includes a binding site for CAD, a small Orai-activating STIM1 C-terminal fragment that interacts with higher affinity also with the C terminus of Orai1 (30). Furthermore, an increased hydrophobicity at the N terminus/membrane interface as present in the SCID mutant Orai1 R91W impairs gating (19). Fast inactivation of Orai1 requires the interaction of CaM with the conserved N-terminal region (16). Hence, multiple

* This work was supported in part by Austrian Science Fund (FWF) Projects P211925 (to K. G.) and P22565 (to C. R.) and Austrian Research Promotion Agency (FFG) Austrian Nanoscience Initiative VO104-08-BI Project 819703 NSI-NABIOS (to H. J. G.).

[S] The on-line version of this article (available at http://www.jbc.org) contains supplemental Figs. 1–6.

⌘ *Author's Choice*—Final version full access.

[1] Both authors contributed equally to this work.

[2] Supported by Hertha-Firnberg Scholarship T466. To whom correspondence may be addressed. E-mail: isabella.derler@jku.at.

[3] Supported by Hertha-Firnberg Scholarship T442.

[4] To whom correspondence may be addressed. Tel.: 43-732-2468-9272; Fax: 43-732-2468-9280; E-mail: christoph.romanin@jku.at.

[5] The abbreviations used are: CRAC, Ca^{2+} release-activated Ca^{2+}; 2-APB, 2-aminoethoxydiphenyl borate; CaM, calmodulin; aa, amino acid(s); CAD, CRAC activation domain; CFP, cyan fluorescent protein; ECFP, enhanced CFP; EYFP, enhanced YFP; I/V, current/voltage.

residues in the N terminus of Orai1 are involved in the gating of the channel.

Here, we examined a series of N-terminal deletion mutants to pinpoint those residues within the N-terminal conserved region of Orai3 that are essential for the gating by STIM1 and 2-APB. Electrophysiological analysis of the Orai3 mutants revealed that increasing N-terminal truncations progressively interfered with fast inactivation, then with STIM1-mediated activation, and finally with 2-APB stimulation.

MATERIALS AND METHODS

Molecular Biology—Human STIM1 (hereafter referred to as STIM1; GenBank™ accession number NM_003156) N-terminally ECFP- and EYFP-tagged was kindly provided by T. Meyer's laboratory, Stanford University. STIM1 C terminus (aa 233–685) was cloned into the T/A site of pcDNA3.1V5 His TOPO (Invitrogen) by PCR and subcloned into pECFP-C1 and pEYFP-C1 (Clontech) via the restriction sites KpnI and XbaI. By introducing a stop codon at amino acid position 475, pECFP-C1 STIM1 233–474 was constructed.

Human Orai3 (Orai3; GenBank accession number NM_152288) was kindly provided by L. Birnbaumer (NIEHS, National Institutes of Health, Research Triangle Park, NC). Orai3 was cloned into the pEYFP-C1 (Clontech) expression vector via its BamHI and XbaI restriction sites also for N-terminal labeling. All Orai3 N-terminal deletion mutants (Orai3 ΔN_{1-46}, ΔN_{1-47}, ΔN_{1-51}, ΔN_{1-53}, ΔN_{1-55}, ΔN_{1-57}, ΔN_{1-58}, ΔN_{1-60}, ΔN_{1-62}, and ΔN_{1-63}) were cloned via PCR into the T/A site of pcDNA3.1V5 His TOPO vector (Invitrogen) and recloned into pEYFP-C1 (Clontech) expression vector via its BamHI and XbaI restriction sites. For the generation of pEYFP-C1 Orai3 R52A/R53A and pEYFP-C1 Orai3 ΔN_{1-51} R52A/R53A mutants, pEYFP-C1 Orai3 and pEYFP-C1 Orai3 ΔN_{1-51} were used as templates, respectively. Suitable primers exchanged the corresponding codons from CGC (Arg) to GCC (Ala). YFP-C1 Orai3 served as a template for the generation of pEYFP-C1 Orai3 ΔR52 ΔR53 and pEYFP-C1 Orai3 R47Q. For the generation of the latter, primers were used that exchanged the corresponding codon from CGG (Arg) to CAG (Gln). In the case of pEYFP-C1 Orai3 ΔR52 ΔR53, primers were designed to delete the corresponding codons CGC (Arg) and CGC (Arg). pEYFP-C1 Orai3 ΔN_{1-55} and pEYFP-C1 Orai3 ΔN_{1-57} served as templates for the generation of pEYFP-C1 Orai3 ΔN_{1-55} L285S/L292S and pEYFP-C1 Orai3 ΔN_{1-57} L285S/L292S mutants, respectively. Suitable primers exchanged the corresponding codons from CTG (Cys) to TCG (Ser). Orai3 ΔN_{1-51} and Orai3 ΔN_{1-53} chimeras both containing the C terminus of Orai1 were cloned via splicing by overlap extension into pcDNA3.1V5 His TOPO vector (Invitrogen) and via the internal restriction sites BamHI and XbaI into the pEYFP-C1 (Clontech) expression vector for N-terminal fluorescence labeling.

C-terminally enhanced GFP-labeled human CRACR2A and mouse CRACR2B were kindly provided by the lab of Yousang Gwack, University of California. cDNA was subcloned into pEYFP/pECFP-C1 vectors (Clontech) via their internal restriction sites BglII and EcoRI. All clones were confirmed by sequence analysis.

Peptide-CaM Binding PAGE Shift Assay—Calmodulin from bovine testes (300 pmol; Sigma) was incubated for 30 min at 21 °C with a variable molar excess of peptides aa 47–65, aa 52–6, or aa 52–65 R52A/R53A (Peptide 2.0 Inc.; derivatized on the additional C-terminal cysteine with biotin-PEG_6-maleimide to prevent disulfide formation; see BIAcore experiments) in incubation buffer (150 mM NaCl, 5 mM HEPES, pH 7.3) together with either 2 mM EGTA or 2 mM Ca^{2+}. Electrophoresis was carried out in 12% polyacrylamide gels in the same buffers under non-denaturing conditions. The gels were stained with Coomassie Blue. Peptides display a highly positive charge at neutral pH (pI between 9.2 and 10.5) and thus have the tendency to migrate to the cathode, which is located on the top of the gel. In the case of an interaction of CaM with a positively charged peptide, this complex would have a larger size and a lower net negative charge than free CaM, resulting in slower migration toward the anode on the bottom of the gel.

Electrophysiology—Electrophysiological recordings comparing characteristics of two to three constructs were carried out in a paired comparison on the same day. Expression patterns and levels of the various constructs were carefully monitored by confocal fluorescence microscopy and were not significantly changed by the introduced mutations. Electrophysiological experiments were performed at 20–24 °C using the patch clamp technique in the whole cell recording configuration. For STIM1/Orai as well as STIM1 C terminus/Orai current measurements, voltage ramps were usually applied every 5 s from a holding potential of 0 mV, covering a range of −90 to +90 mV over 1 s. The internal pipette solution for passive store depletion contained 3.5 mM $MgCl_2$, 145 mM cesium methanesulfonate, 8 mM NaCl, 10 mM HEPES, 20 mM EGTA, pH 7.2. The 100 nM Ca^{2+} containing intracellular solution included 3.5 mM $MgCl_2$, 145 mM cesium methanesulfonate, 8 mM NaCl, 10 mM HEPES, 10 mM EGTA, 4.3 mM $CaCl_2$, pH 7.2. Extracellular solution consisted of 145 mM NaCl, 5 mM CsCl, 1 mM $MgCl_2$, 10 mM HEPES, 10 mM glucose, 10 mM $CaCl_2$, pH 7.4.

Confocal Fluorescence Microscopy—Confocal microscopy for co-localization experiments was performed similarly as described (32). In brief, a QLC100 Real-Time Confocal System (VisiTech International) connected to two Photometrics CoolSNAPHQ monochrome cameras (Roper Scientific) and a dual port adapter (dichroic, 505lp; cyan emission filter, 485/30 nm; yellow emission filter, 535/50 nm; Chroma Technology Corp.) was used for recording fluorescence images. This system was attached to an Axiovert 200M microscope (Zeiss) in conjunction with an argon ion multiwavelength (457, 488, and 514 nm) laser (Spectra Physics). The wavelengths were selected by an Acousto Optical Tuneable Filter (VisiTech International). MetaMorph 5.0 software (Universal Imaging Corp.) was used to acquire images and to control the confocal system. Illumination times for CFP and YFP images that were recorded with a minimum delay consecutively were about 900 ms.

BIAcore—Specific binding of calmodulin to N-terminal Orai peptides was measured by surface plasmon resonance in a BIAcore X setup at 25 °C. The Orai peptides were custom synthesized (Peptide 2.0 Inc.) with an extra cysteine on their C terminus (as amide with ammonia). The C-terminal cysteine

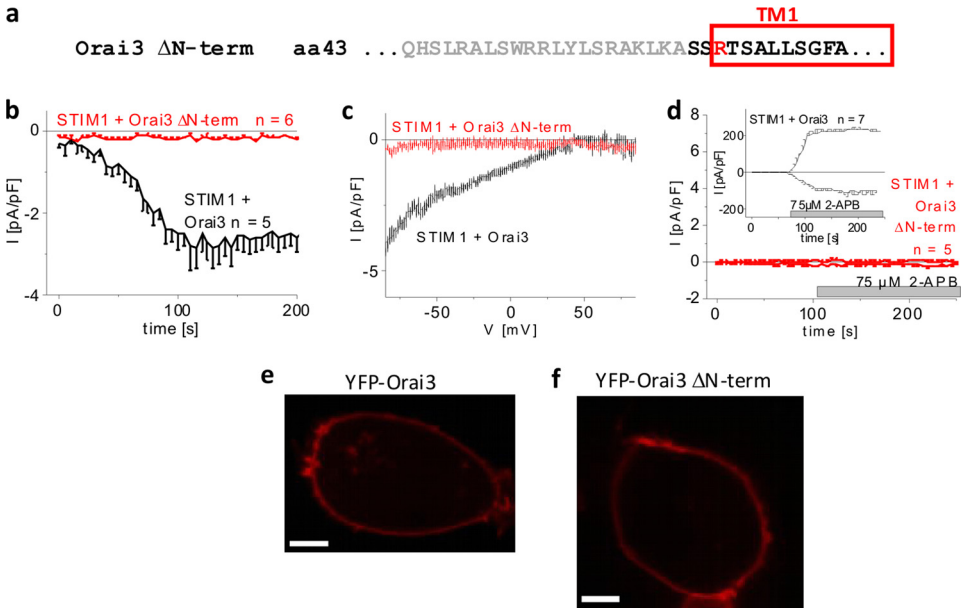

FIGURE 1. **Deletion of whole N terminus (aa 1–63) of Orai3 disrupts its activation.** *a*, amino acid sequence of Orai3 ΔN-term deletion mutant. *Gray letters* represent amino acids within the N terminus of Orai3 that were deleted. *b*, time course of whole cell inward currents at −74 mV activated by passive store depletion of HEK 293 cells coexpressing CFP-STIM1 and YFP-Orai3 ΔN-term in comparison with wild-type YFP-Orai3 ($p < 0.01$). *c*, current/voltage relationship corresponding to *b*. *d*, time course of whole cell currents at −74 and +74 mV of HEK 293 cells coexpressing CFP-STIM1 and YFP-Orai3 ΔN-term upon perfusion with 75 μM 2-APB ($p < 0.01$). Confocal fluorescence images from a representative cell expressing wild-type YFP-Orai3 (*e*) and YFP-Orai3 ΔN-term (*f*) are shown. *Bars* in fluorescence images correspond to 5 μm. *pF*, picofarad. *Error bars* represent S.E.

was coupled to maleimide-PEG_8-biotin[6] using a slight excess of tris(2-carboxyethyl)phosphine for *in situ* reduction of potentially oxidized peptides as well as 1 mM EDTA and an argon atmosphere to prevent reoxidation. The biotin-PEG-peptide conjugates were purified by reversed phase chromatography, and the structures were confirmed by MALDI-TOF mass spectrometry. The biotin-PEG-peptide conjugates were bound to streptavidin-functionalized surface plasmon resonance chips by injection into flow cell 1 but only after the streptavidin molecules in flow cell 2 (control cell) had been blocked with an excess of free biotin (see legends to supplemental Figs. 4 and 5). The chips were superfused with HEPES buffer (150 mM NaCl, 5 mM HEPES, pH 7.3) at a constant rate of 20 μl/min. Binding of CaM was tested by injecting the protein (2 μM) in HEPES buffer containing either 2 mM $CaCl_2$ or 2 mM EGTA and recording the surface plasmon resonance angle in both flow cells.

RESULTS

Deletion of Whole N Terminus of Orai3 Disrupts Its Activation—Because Orai3 channels can be stimulated by store depletion as well as 2-APB, we utilized both modes of activation to investigate the role of the N terminus in the Orai3 gating machinery. Initially, we generated an N-terminally YFP-labeled Orai3 deletion mutant lacking the complete N terminus (Orai3 ΔN-term = ΔN_{1-63}) (Fig. 1*a*). Coexpression of CFP-STIM1 and YFP-Orai3 ΔN-term revealed a lack of current activation following passive store depletion by 20 mM EGTA (Fig. 1, *b* and *c*) in close analogy to previous reports with the corresponding Orai1 ΔN_{1-88} deletion mutant (10, 27). The Orai3-specific 2-APB stimulation was similarly disrupted by the full N-terminal truncation (Fig. 1*d*). Using confocal fluorescence microscopy, we observed a comparable level of plasma membrane expression for both the wild type (Fig. 1*e*) and the Orai3 N-terminal deletion mutant (Fig. 1*f*). Moreover, the deletion mutant showed the same ability to homomultimerize as deduced from FRET measurements of cells expressing YFP- and CFP-labeled Orai3 ΔN-term (data not shown). Hence, the full N terminus of Orai3 or at least a portion of it is indispensable for both STIM1- and 2-APB-mediated Orai3 activation.

Progressive Truncations until Residues 48–51 Differentially Affect Activation and Inactivation of Orai3 Currents—The Orai3 N terminus contains a region (aa 48–65) proximal to the first transmembrane domain that is fully conserved among all Orai proteins (supplemental Fig. 1). An N-terminal deletion until aa 73 in Orai1 (corresponding to aa 48 in Orai3) maintains store-operated activation but to a reduced extent (27). Hence, it has been hypothesized that the fully conserved region is essential for Orai1 activation (27, 29). We examined this hypothesis for Orai3 by generating a series of N-terminal deletion mutants and analyzing their overall gating behavior in terms of activation and inactivation using either STIM1 or 2-APB as the activating stimulus. In a first step, we investigated Orai3 N-terminal deletion mutants lacking 46, 47, 49, and 51 amino acids (Orai3 ΔN_{1-46}, ΔN_{1-47}, ΔN_{1-49}, and ΔN_{1-51}) (Fig. 2*a*). Although the Orai3 ΔN_{1-46} and ΔN_{1-47} mutants still contain the full conserved region (supplemental Fig. 1), the Orai3 ΔN_{1-49} and ΔN_{1-51} mutants lack the first two (Ala^{48}-Leu^{49}) and four (Ala^{48}-Leu^{49}-Ser^{50}-Trp^{51}) amino acids of the conserved domain. Orai3 ΔN_{1-46}, ΔN_{1-47}, and ΔN_{1-49} displayed store-operated activation to an extent comparable with wild type, and the Orai3 ΔN_{1-51} mutant exhibited slightly reduced currents (Fig. 2, *b*, *e*, and *k*, and supplemental Fig. 3a). All four deletion mutants showed similar current/voltage characteris-

[6] P. Pollheimer, A. Scherflér, P. Wiesauer, C. Schwarzinger, and H. J. Gruber, manuscript in preparation.

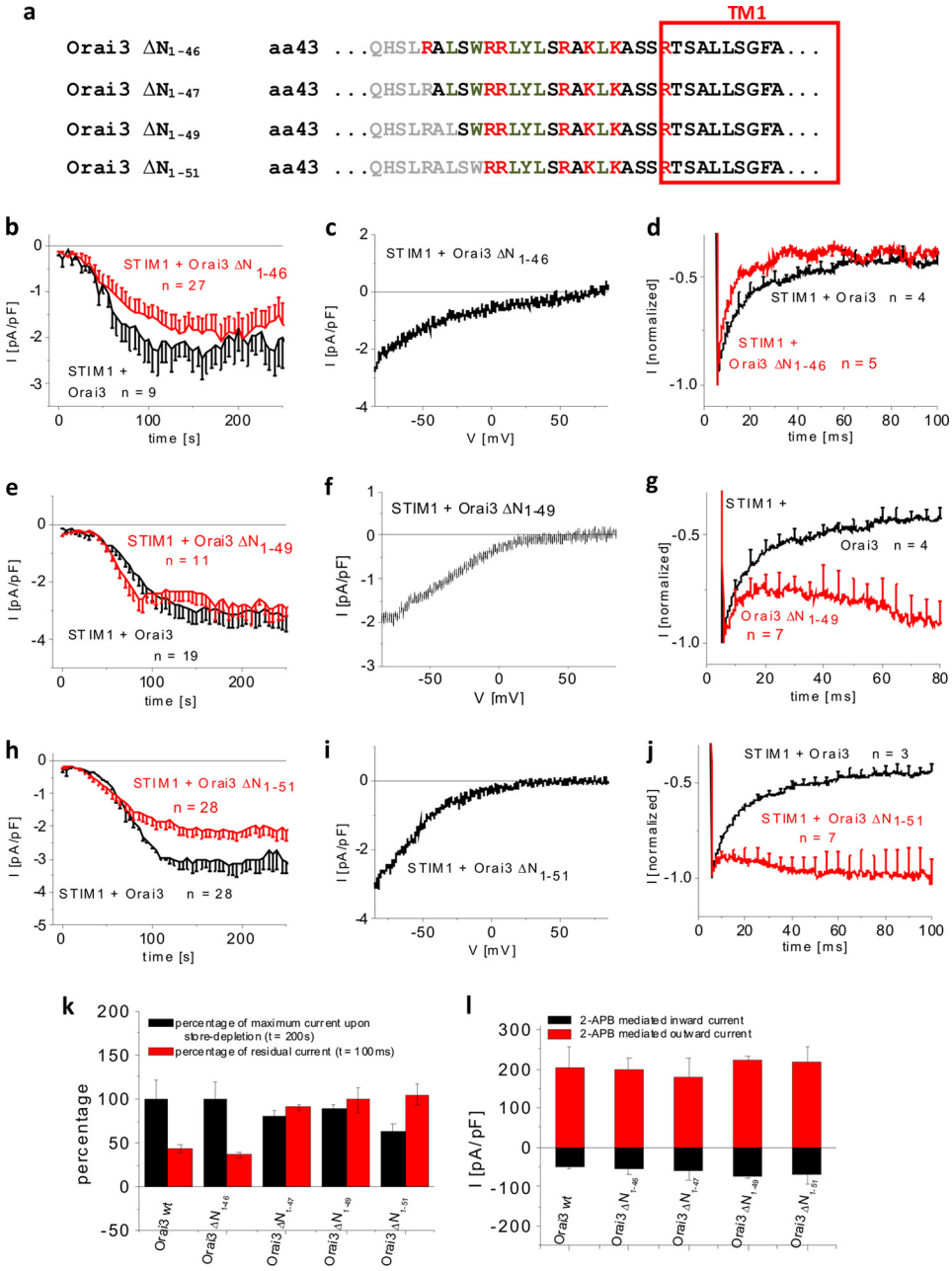

FIGURE 2. **Store-operated activation is retained upon deletion of first four amino acids of N-terminal conserved region of Orai3.** *a*, amino acid sequence of Orai3 N-terminal deletion mutants. *Gray letters* represent amino acids within the N terminus of Orai3 that were deleted. Shown are times course of whole cell inward currents at −74 mV activated by passive store depletion of HEK 293 cells coexpressing CFP-STIM1 with YFP-Orai3 ΔN_{1-46} (*b*), YFP-Orai3 ΔN_{1-49} (*e*), and YFP-Orai3 ΔN_{1-51} (*h*) in comparison with wild-type YFP-Orai3. *c*, *f*, and *i*, current/voltage relationship corresponding to *b*, *e*, and *h*, respectively. The mean fast inactivation for 100 ms upon voltage steps from a holding potential of 0 to −90 mV of normalized current traces of CFP-STIM1-mediated YFP-Orai3 ΔN_{1-46} (*d*), YFP-Orai3 ΔN_{1-49} (*g*), and YFP-Orai3 ΔN_{1-51} (*j*) currents is shown. *k*, block diagram opposing the percentage of maximal store-operated currents ($t = 200$ s) against the percentage of residual currents after 100 ms upon application of a voltage step to −90 mV of Orai3 and Orai3 deletion mutants (for Orai3 ΔN_{1-46}, $p > 0.05$ for store-operated currents at $t = 200$ s as well as residual currents of inactivation at $t = 100$ ms; for Orai3 ΔN_{1-47}, ΔN_{1-49}, and ΔN_{1-51}, $p > 0.05$ for store-operated currents at $t = 200$ s but $p < 0.05$ for residual currents of inactivation at $t = 100$ ms) mentioned in this figure. *l*, block diagram of whole cell inward (−74 mV) and outward (+74 mV) currents of HEK 293 cells coexpressing CFP-STIM1 with YFP-Orai3 ΔN_{1-46}, YFP-Orai3 ΔN_{1-47}, YFP-Orai3 ΔN_{1-49}, and YFP-Orai3 ΔN_{1-51} upon perfusion with 75 μM 2-APB (for inward as well as outward currents at $t = 100$ s upon application of 2-APB, $p > 0.05$). *pF*, picofarad. *Error bars* represent S.E.

tics (Fig. 2, *c*, *f*, and *i*, and supplemental Fig. 3b). Confocal fluorescence microscopy indicated comparable plasma membrane localization of all four Orai3 deletion mutants (supplemental Fig. 2, a–h). The smaller current size of Orai3 ΔN_{1-51} was probably not due to reduced plasma membrane expression as 75 μM 2-APB stimulated the four deletion mutants to levels similar to that of wild-type Orai3 (Fig. 2*l* and supplemental Fig. 3g) consistent with their overall comparable plasma membrane expression. Analysis of the inactivation behavior revealed that the Orai3 ΔN_{1-46} mutant displayed strong, fast inactivation during a voltage step to −90 mV equivalent to wild-type Orai3 (Fig. 2*d* and supplemental Fig. 3j), whereas the shorter truncation mutants exhibited currents with substantial attenuation of inactivation (Fig. 2, *g*, *j*, and *k*, and supplemental Fig. 3, c and k).

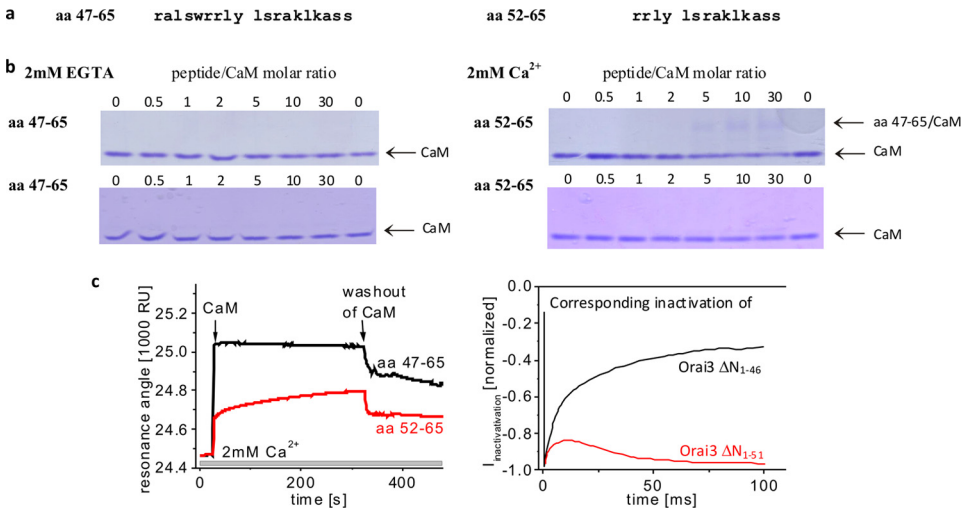

FIGURE 3. **Interaction of Orai3 N terminus with CaM.** *a*, amino acid sequence of two Orai3 N-terminal peptides, aa 47–65 and aa 52–65. *b*, PAGE shift assay demonstrating Ca^{2+} dependence of CaM interaction with peptides aa 47–65 and aa 52–65 in 2 mM EGTA and 2 mM Ca^{2+} media at different peptide/CaM ratios. *c*, BIAcore sensorgrams displaying binding of CaM to peptide aa 47–65 compared with that of aa 52–65 in the presence of 2 mM Ca^{2+}. On the *right side*, inactivation profiles of Orai3 ΔN_{1-46} and Orai3 ΔN_{1-51} are shown in accordance with the respective sensorgrams. *RU*, resonance units.

Furthermore, deletion of the arginine Arg^{47} significantly reduced inactivation, and continuative truncations until Trp^{51} led to further gradual loss of fast inactivation. A comparison of maximum current densities reached at 200 s and inactivation represented by normalized residual currents at 100 ms (Fig. 2*k*) showed no general correlation between the current amplitudes and the extent of inactivation among these mutants. In summary, N-terminal aa 47–51 represent key residues for fast inactivation of Orai3 truncation mutants but are not essential for Orai3 activation via STIM1 or 2-APB.

Diminished Inactivation of Orai3 N-terminal Deletion Mutants Correlates with Reduced Calmodulin Binding—Mullins *et al.* (16) have reported that disruption of the CaM-binding domain within Orai1 N terminus by single point mutations results in reduced fast inactivation. We have recently demonstrated that CaM dynamically interacts in a Ca^{2+}-dependent manner with the N terminus of Orai1 as well as Orai3 (14). The CaM-binding domain is located in the aa 67–82 stretch in Orai1 that corresponds to aa 43–62 in Orai3 (supplemental Fig. 1). This region overlaps with the N-terminal region (aa 48–65 in Orai3) that is conserved among all Orai isoforms. In an attempt to relate the reduction of inactivation of the Orai3 ΔN_{1-47} and shorter deletion mutants to a reduced CaM binding, we carried out native PAGE shift assays of CaM in the presence of the respective peptides. The two synthetic peptides, aa 47–65 and aa 52–65 (Fig. 3*a*), were designed to mimic CaM binding of the corresponding Orai3 ΔN_{1-46} and Orai3 ΔN_{1-51} channels that exhibited distinct fast inactivation. PAGE shift assays were carried out under non-denaturing conditions following preincubation of CaM with increasing amounts of peptides either in the absence (2 mM EGTA) or in the presence (2 mM Ca^{2+}) of Ca^{2+}. In the absence of Ca^{2+}, the CaM bands remained comparably intense for both peptides independently of the peptide/CaM ratio as expected for the absence of peptide-CaM interaction (16) (Fig. 3*b*, *left*). In the presence of Ca^{2+}, the CaM band displayed a progressive reduction of intensity, starting at a ratio of 5 for aa 47–65/CaM (Fig. 3*b*, *upper right*), together with the appearance of a second, weak band that likely corresponds to the peptide-CaM complex. The shorter peptide, aa 52–65, displayed almost no reduction of the CaM band with increasing peptide/CaM ratios (Fig. 3*b*, *lower right*). To quantitatively address the interaction of CaM with these two peptides, we additionally carried out BIAcore experiments. For this purpose, the C terminus of the peptides was extended with a hexa(ethylene glycol) linker carrying a terminal biotin group. The biotinylated peptide was immobilized on a streptavidin-functionalized sensor chip in flow cell 1, whereas the streptavidin molecules in the parallel flow cell 2 were blocked with free D-biotin. Both flow cells were perfused in series with buffer containing 2 mM EGTA or 2 mM Ca^{2+} before injecting 2 μM CaM either in Ca^{2+}-free buffer or in Ca^{2+} buffer, respectively.

Consistent with Park *et al.* (30) and results obtained by the PAGE shift assays above, BIAcore experiments revealed no CaM binding for any peptide in the presence of EGTA (data not shown). In a 2 mM Ca^{2+}-containing buffer, however, we observed a stronger as well as faster binding of CaM to the longer peptide (450 resonance units) compared with the shorter peptide (207 resonance units) (Fig. 3*c*, *left*). Thus, the distinct Ca^{2+}-dependent CaM binding capabilities of the aa 47–65 and aa 52–65 peptides correlated well with the degree of inactivation of the Orai3 ΔN_{1-46} and Orai3 ΔN_{1-51} channels, respectively (Fig. 3*c*, *right*). Presumably, the progressive deletion of the Orai3 N terminus from aa 46 to 51 gradually decreases CaM binding, which is reflected in a successive attenuation of Orai3 inactivation.

Arginines at Positions 52/53 Exert Inhibitory Effect on Orai3 Gating—Mapping of the remaining residues in the conserved Orai3 N-terminal region was continued by generating further Orai3 deletion mutants, Orai3 ΔN_{1-53} and ΔN_{1-55} (Fig. 4*a*). The Orai3 ΔN_{1-53} lacked the two positively charged arginines $Arg^{52/53}$, and the Orai3 ΔN_{1-55} additionally lacked the subsequent two hydrophobic amino acids. Both mutants exhibited well preserved store-operated activation with current densities

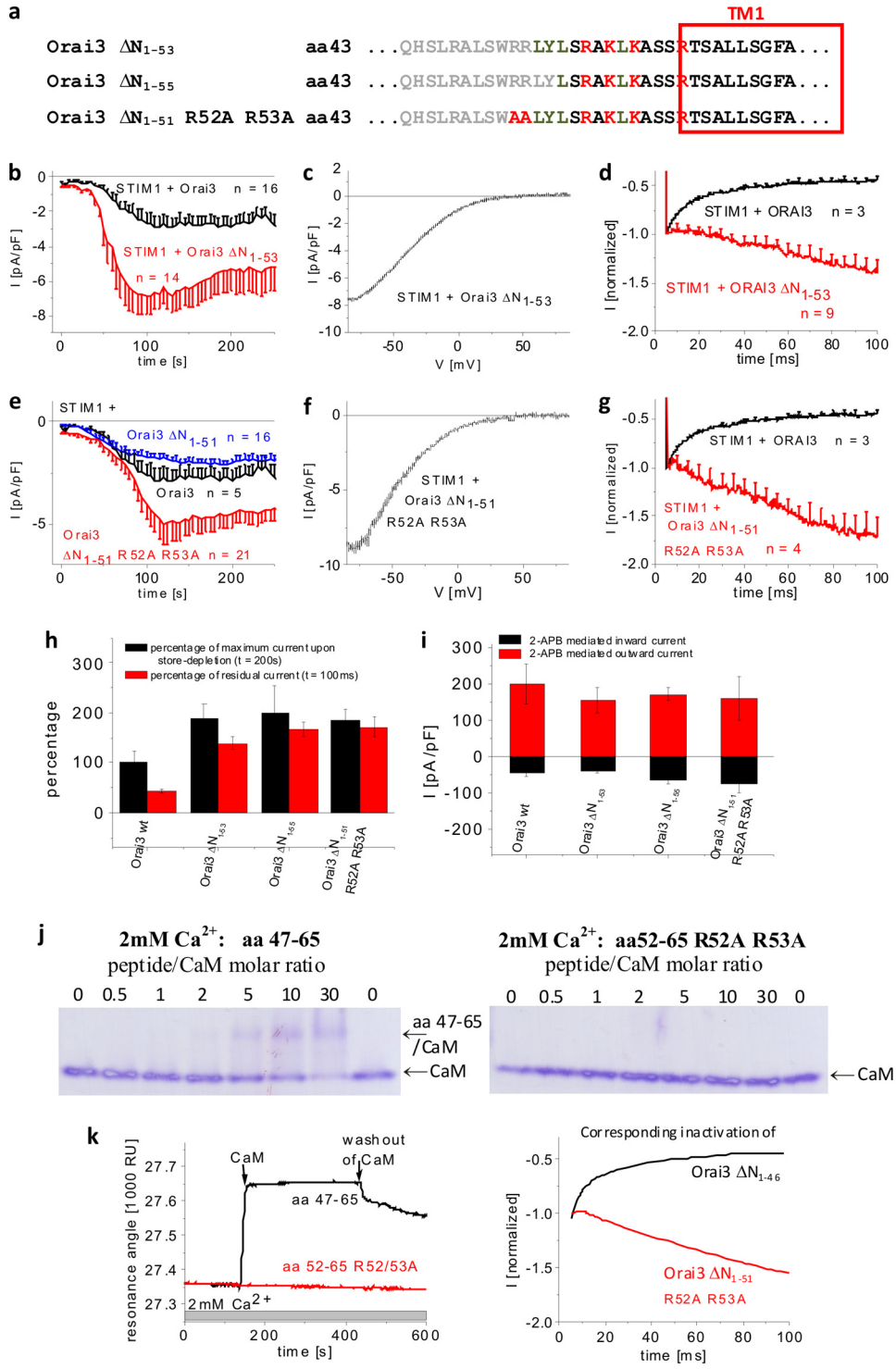

FIGURE 4. **Two arginines exert inhibitory effect on Orai3 gating.** *a*, amino acid sequence of Orai3 N-terminal deletion mutants. *Gray letters* represent amino acids within the N terminus of Orai3 that were deleted. Shown are time courses of whole cell inward currents at −74 mV activated by passive store depletion of HEK 293 cells coexpressing CFP-STIM1 with YFP-Orai3 ΔN_{1-53} (*b*) and YFP-Orai3 ΔN_{1-51} R52A/R53A (*e*) in comparison with wild-type Orai3 (*b*) and in comparison with both wild-type Orai3 and YFP-Orai3 ΔN_{1-51} (*e*). *c* and *f*, current/voltage relationships corresponding to *b* and *e*, respectively. The mean fast inactivation for 100 ms upon voltage steps from a holding potential of 0 to −90 mV of normalized current traces of CFP-STIM1-mediated YFP-Orai3 ΔN_{1-53} (*d*) and YFP-Orai3 ΔN_{1-51} R52A/R53A (*g*) currents in comparison with wild-type YFP-Orai3. *h*, block diagram opposing the percentage of maximal store-operated currents ($t = 200$ s) against the percentage of residual currents after 100 ms upon application of a voltage step to −90 mV of Orai3 and the Orai3 deletion mutants indicated ($p < 0.01$ for store-operated currents at $t = 200$ s as well as residual currents of inactivation at $t = 100$ ms). *i*, block diagram of whole cell inward (−74 mV) and outward (+74 mV) currents of HEK 293 cells coexpressing CFP-STIM1 with YFP-Orai3 ΔN_{1-53}, YFP-Orai3 ΔN_{1-55}, and YFP-Orai3 ΔN_{1-51} R52A/R53A upon perfusion with 75 μM 2-APB (for inward as well as outward currents at $t = 100$ s upon application of 2-APB, $p > 0.05$). *j*, PAGE shift assay demonstrating Ca^{2+} dependence of CaM interaction with peptides aa 47–65 and aa 52–65 R52A/R53A in 2 mM Ca^{2+} medium at different peptide/CaM ratios. *k*, BIAcore sensorgrams displaying binding of CaM to peptide aa 47–65 compared with aa 52–65 R52A/R53A in the presence of 2 mM Ca^{2+}. On the *right side*, inactivation profiles of Orai3 ΔN_{1-46} and Orai3 ΔN_{1-51} R52A/R53A are shown in accordance with the respective sensorgrams. *pF*, picofarad; *RU*, resonance units. *Error bars* represent S.E.

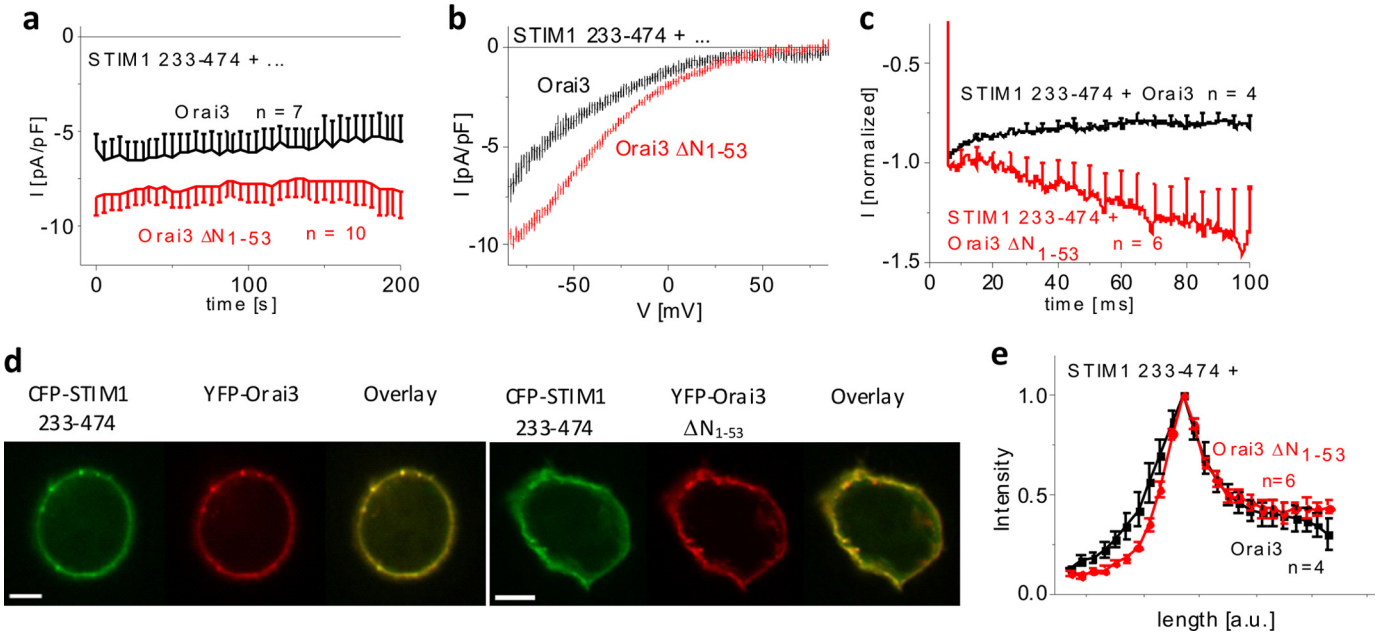

FIGURE 5. **N-truncated Orai3 mutants with potentiated currents exhibit coupling similar to STIM1.** *a*, time course of constitutive whole cell inward currents at −74 mV of HEK 293 cells coexpressing CFP-STIM1 233–474 with YFP-Orai3 ΔN_{1-53} in comparison with wild-type YFP-Orai3 ($t = 0$ s, $p < 0.05$). *b*, current/voltage relationships corresponding to *a*. *c*, mean fast inactivation for 100 ms upon voltage steps from a holding potential of 0 to −90 mV of normalized current traces of CFP-STIM1 233–474-mediated Orai3 ΔN_{1-53} currents compared with Orai3 currents ($t = 0$ s, $p < 0.05$). *d*, localization and overlay of CFP-STIM1 233–474 and YFP-Orai3 or YFP-Orai3 ΔN_{1-53}. *e*, intensity plots representing the localization of STIM1 233–474 across the cell when coexpressed with Orai3 ΔN_{1-53} compared with wild-type Orai3. *Bars* in fluorescence images correspond to 5 μm. *pF*, picofarad; *a.u.*, arbitrary units. *Error bars* represent S.E.

that were more than 2-fold increased compared with that of Orai3 wild-type (Fig. 4, *b* and *h*, and supplemental Fig. 3d). Confocal fluorescence microscopy images displayed plasma membrane localization for Orai3 ΔN_{1-53} and Orai3 ΔN_{1-55} equivalent to wild-type Orai3 (supplemental Fig. 2). Accordingly, 75 μM 2-APB stimulated Orai3 ΔN_{1-53} and ΔN_{1-55} currents to levels similar to that of wild-type Orai3 (Fig. 3*i* and supplemental Fig. 3h) consistent with their similar levels of plasma membrane expression. Strikingly, their current/voltage (I/V) relationships displayed U-shaped characteristics at negative potentials (Fig. 4*c* and supplemental Fig. 3e) that were not visible for Orai3 inward currents. Voltage steps for both Orai3 ΔN_{1-53} and ΔN_{1-55} channels revealed substantial current potentiation without any Ca^{2+}-dependent inactivation over the first 100 ms (Fig. 4, *d* and *g*, and supplemental Fig. 3, f and l). The current potentiation of these mutants likely resulted in the U-shaped I/V relationship and the increased maximum currents, suggesting a profound gating effect.

We hypothesized that the two arginines at positions 52 and 53 might affect Orai3 gating. Mutating these two arginines to alanines in the Orai3 ΔN_{1-51} R52A/R53A mutant indeed increased currents 2–3-fold (Fig. 4, *e* and *h*) and yielded a U-shaped I/V relationship (Fig. 4*f*) similar to that of Orai3 ΔN_{1-53}. 2-APB currents of this double point mutant developed to levels comparable with wild-type Orai3 levels (Fig. 4*i*) consistent with similar plasma membrane expression (supplemental Fig. 2). In accordance with Orai3 ΔN_{1-53} and Orai3 ΔN_{1-55}, Orai3 ΔN_{1-51} R52A/R53A displayed a pronounced potentiation during a voltage step to −90 mV (Fig. 4*g* and supplemental Fig. 3*l*). Thus, gating of the Orai3 ΔN_{1-51} R52A/R53A mutant (Fig. 4*g*) looked equivalent to that of Orai3 $\Delta N_{1-53/55}$, indicating a modulatory role of the two arginines Arg^{52}-Arg^{53} in the gating of the Orai3 truncation mutant. The complete absence of fast inactivation in the Orai3 ΔN_{1-51} R52A/R53A or Orai3 $\Delta N_{1-53/55}$ mutant might be caused by abrogated CaM binding, which is still visible with the Orai3 ΔN_{1-51}-mimicking peptide. Native PAGE shift assays with CaM and the peptide aa 52–65 R52A/R53A, corresponding to Orai3 ΔN_{1-51} R52A/R53A, did not display a change in CaM bands with increasing peptide/CaM ratio (Fig. 4*j*). Moreover, BIAcore experiments failed to detect significant binding of CaM to aa 52–65 R52A/R53A (Fig. 4*k*) contrary to the other two peptides mentioned in the previous section. In summary, $\Delta N_{1-53/55}$ deletions or mutation of Arg^{52}-Arg^{53} within ΔN_{1-51} altered Orai3 gating by increasing maximum Orai3 currents and concomitantly reversed inactivation into potentiation. This potentiation was accompanied by a complete disruption of CaM binding.

N-truncated Orai3 Mutants with Potentiated Currents Exhibit Coupling Similar to STIM1—Because STIM1-mediated Orai3 $\Delta N_{1-53/55}$ currents were strongly increased, we examined the impact of the truncated N terminus on the coupling to STIM1. To reveal a potential change in affinity, we utilized the STIM1 233–474 cytosolic fragment as a surrogate for STIM1. Orai3 $\Delta N_{1-53/55}$ currents that were constitutively activated by STIM1 233–474 displayed enhanced current densities and slightly U-shaped I/V relationships (Fig. 5, *a* and *b*) as compared with wild-type Orai3. In line with the experiments with full-length STIM1, the slight inactivation of Orai3 currents changed into a strong potentiation with Orai3 ΔN_{1-53} when stimulated by STIM1 233–474 (Fig. 5*c*). Hence, the observed effects of STIM1 233–474 fragment were comparable with those obtained with full-length STIM1. The enhanced currents of Orai3 $\Delta N_{1-53/55}$ less likely resulted from increased interaction with STIM1 as co-localization and intensity profiles of STIM1

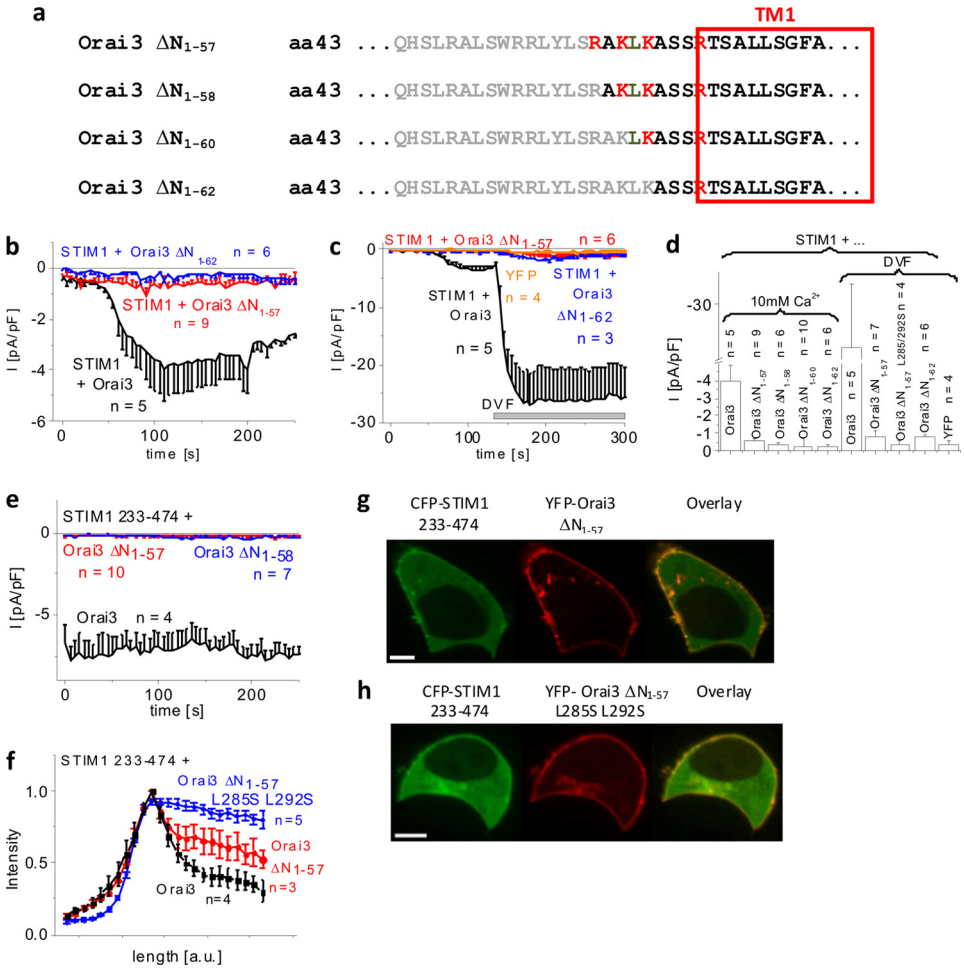

FIGURE 6. **N-terminal deletions until position 57 or further significantly diminish store-operated Orai3 activation.** *a*, amino acid sequence of Orai3 N-terminal deletion mutants. *Gray letters* represent amino acids within the N terminus of Orai3 that were deleted. *b*, time course of whole cell inward currents at −74 mV activated by passive store depletion of HEK 293 cells coexpressing CFP-STIM1 with YFP-Orai3 ΔN_{1-57} and YFP-Orai3 ΔN_{1-62} in comparison with wild-type YFP-Orai3. *c*, time course of whole cell inward currents at −74 mV upon perfusion with divalent cation-free (*DVF*) solution of HEK 293 cells expressing YFP or coexpressing CFP-STIM1 with YFP-Orai3, YFP-Orai3 ΔN_{1-57}, or YFP-Orai3 ΔN_{1-62}. *d*, block diagram comparing maximal currents in 10 mM Ca^{2+} of HEK cells coexpressing CFP-STIM1 and YFP-Orai3, YFP-Orai3 ΔN_{1-57}, YFP-Orai3 ΔN_{1-58}, YFP-Orai3 ΔN_{1-60}, or YFP-Orai3ΔN_{1-62} ($p < 0.05$) as well as in divalent cation-free (*DVF*) solution of HEK 293 cells expressing YFP or coexpressing CFP-STIM1 and YFP-Orai3, YFP-Orai3 ΔN_{1-57}, YFP-Orai3 ΔN_{1-57} L285S/L292S, or YFP-Orai3 ΔN_{1-62} ($p < 0.05$). *e*, time course of whole cell inward currents at −74 mV activated by passive store depletion of HEK 293 cells coexpressing CFP-STIM1 233–474 with YFP-Orai3 ΔN_{1-57} and YFP-Orai3 ΔN_{1-58} in comparison with wild-type YFP-Orai3 ($p < 0.05$). *f*, intensity plots representing the localization of CFP-STIM1 233–474 across the cell when coexpressed with YFP-Orai3 ΔN_{1-57} L285S/L292S compared with YFP-Orai3 ΔN_{1-57} and wild-type Orai3. *g* and *h*, localization and overlay of CFP-STIM1 233–474 and YFP-Orai3, YFP-Orai3 ΔN_{1-57}, or YFP-Orai3 ΔN_{1-57} L285S/L292S. *Bars* in fluorescence images correspond to 5 μm. *pF*, picofarad. *Error bars* represent S.E.

233–474 with wild-type Orai3 or Orai3 ΔN_{1-53} were similar (Fig. 5, *d* and *e*). Hence, we suggest that the observed biophysical characteristics of Orai3 $\Delta N_{1-53/55}$ result rather from an altered gating than from enhanced STIM1 binding.

Continuative N-terminal Truncations Impair STIM1-mediated Activation of Orai3—Deletion of nearly half of the N-terminal conserved region (aa 48–55) in Orai3 maintained store-operated activation and additionally affected current density and inactivation. To pinpoint the region within the remaining N terminus of Orai3 essential for STIM1-dependent activation, we carried out further truncations, generating Orai3 ΔN_{1-57}, Orai3 ΔN_{1-58}, Orai3 ΔN_{1-60}, and Orai3 ΔN_{1-62} deletion mutants (Fig. 6*a*). All of these mutants still exhibited plasma membrane localization as judged from confocal fluorescence microscopy images (supplemental Fig. 2). Quantitative evaluation of membrane fluorescence intensities exemplarily compared for Orai3 wild type and Orai3 ΔN_{1-47} and Orai3 ΔN_{1-57} mutants only revealed a slight reduction by about 30% for Orai3 ΔN_{1-57} (supplemental Fig. 2i). However, all of the truncation mutants from Orai3 ΔN_{1-57} to Orai3 ΔN_{1-62}, when coexpressed with STIM1, completely lacked store-operated activation (Fig. 6, *b* and *d*, and supplemental Fig. 3i), suggesting that these deletions fully abolished function but not plasma membrane localization. In support of this hypothesis, the application of divalent cation-free solution, which typically amplified wild-type Orai3 currents ~8-fold, resulted in no significant current increases with Orai3 ΔN_{1-57} and ΔN_{1-62} mutants (Fig. 6, *c* and *d*). As additional controls, the Orai3 ΔN_{1-57} L285S/L292S mutant with disrupted STIM1 coupling (24) or YFP-expressing cells displayed similar, marginal increases of the currents in divalent cation-free solution (Fig. 5*d*). The shorter C-terminal STIM1 fragment 233–474 (Fig. 6*e*), which typically exhibits enhanced interaction with Orai proteins and efficient stimulation of Orai currents (28, 30, 33), also failed to evoke significant

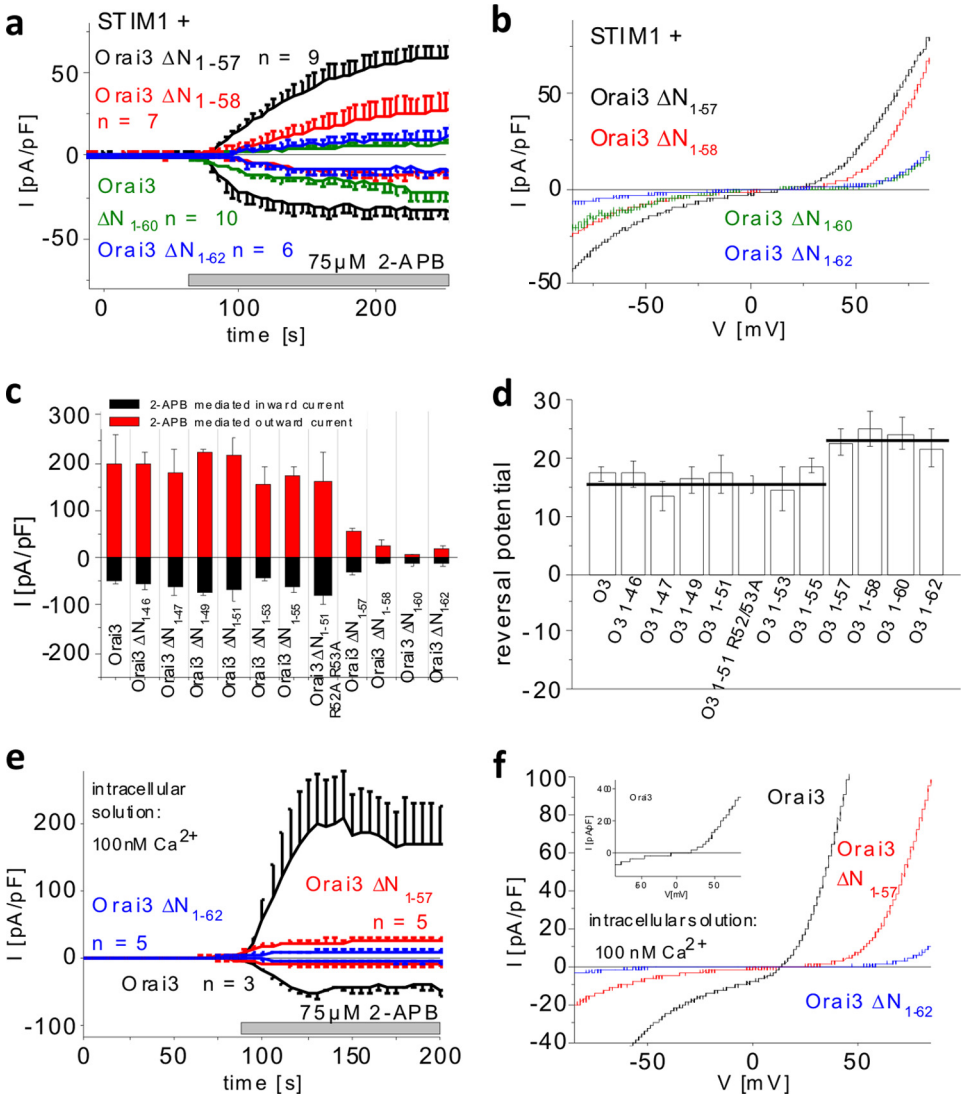

FIGURE 7. **Amino acids 58–62 of Orai3 N terminus are sufficient for 2-APB activation that is independent of STIM1.** *a*, time course of whole cell currents at −74 and +74 mV of HEK 293 cells coexpressing CFP-STIM1 with YFP-Orai3 ΔN_{1-57}, YFP-Orai3 ΔN_{1-58}, YFP-Orai3 ΔN_{1-60}, or YFP-Orai3 ΔN_{1-62} upon perfusion with 75 μM 2-APB ($p < 0.05$). *b*, current/voltage relationships corresponding to *a*. Block diagrams comparing inward and outward currents upon 2-APB stimulation (*c*) and reversal potential of double rectifying 2-APB currents of all Orai3 (*O3*) deletion mutants (Orai3 ΔN_{1-46}–Orai3 ΔN_{1-55}, $p > 0.05$; Orai3ΔN_{1-57}–Orai3 ΔN_{1-62}, $p < 0.05$) (*d*). *e*, time course of whole cell currents at −74 and +74 mV of HEK cells coexpressing CFP-STIM1 and YFP-Orai3, YFP-Orai3 ΔN_{1-57}, or YFP-Orai3 ΔN_{1-62} in the presence of 100 nM Ca^{2+} in the intracellular solution and upon perfusion with 75 μM 2-APB (2-APB currents of respective Orai3 proteins in the presence of 10 mM EGTA compared with 100 nM Ca^{2+} intracellular solution, $p > 0.05$ at $t = 100$ s upon addition of 2-APB). *f*, current/voltage relationship corresponding to *e*. *pF*, picofarad. *Error bars* represent S.E.

currents from these Orai3 deletion mutants. Therefore, we further examined whether the abolished store-operated currents might result from a lack of coupling of the Orai3 ΔN_{1-57} and ΔN_{1-62} mutants with STIM1. Co-localization experiments and density profiles showed a weaker interaction of STIM1 233–474 with Orai3 ΔN_{1-57} than with wild-type Orai3 that was still stronger than with the STIM1-disrupted coupling mutant Orai3 ΔN_{1-57} L285S/L292S (Figs. 6, *f–h*, and 5*d*) (24). Hence, Orai3 channel activation requires, in addition to STIM1 coupling to its C terminus, the presence of an additional N-terminal region upstream to aa 56 as an essential molecular determinant for STIM1-mediated Orai3 current activation.

Orai3 Mutants Lacking Store-operated Activation Are Still Stimulated by 2-APB—Because truncations beyond residue 57 in the Orai3 N terminus abolished store-operated activation, we examined their impact on stimulation by 2-APB. All four deletion mutants, *i.e.* Orai3 ΔN_{1-57}, ΔN_{1-58}, ΔN_{1-60}, and ΔN_{1-62}, that lacked store-operated activation still displayed a current response to 2-APB characterized by double rectifying current/voltage relationships (Fig. 7, *a* and *b*). The mean current densities, however, exhibited significantly reduced levels compared with wild-type Orai3 with the outward currents being more strongly diminished than the inward currents (Fig. 7, *b* and *c*). Close inspection of the I/V relationship revealed a right-shifted reversal potential in comparison with wild-type Orai3 determined at maximum 2-APB currents (Fig. 7*d*). The deletion mutants were also stimulated by 2-APB without coexpression of STIM1 (data not shown). To eliminate a potential effect of endogenous STIM1 contributing to current stimulation, we additionally performed experiments with a 100 nM Ca^{2+} intracellular solution to prevent store depletion. Under these conditions, the 2-APB-activated currents of Orai3, Orai3 ΔN_{1-57},

and Orai3 ΔN_{1-62} developed to an extent similar to that in the presence of passive store depletion (Fig. 7, *e* and *f*). Thus, the second half (aa 56–62) of the conserved region within the Orai3 N terminus is sufficient for 2-APB activation. However, additional amino acids before residue 57 are required for maximum stimulation of Orai3 currents via 2-APB.

DISCUSSION

The present study highlights the versatile role of the N-terminal conserved region (aa 48–65) in the gating of Orai3 channels. Distinct molecular determinants were identified for Orai3 activation by STIM1 and 2-APB. Moreover, fast inactivation of Orai3 channels mediated by CaM binding was reversed into strong potentiation upon partial truncation of the conserved N-terminal region.

Utilizing a detailed series of N-terminal truncation mutants of Orai3, we confined the minimal essential domain for STIM1-mediated activation to the second half (aa 56–65) of the N-terminal conserved region of Orai3. Further truncations beyond aa 57 resulted in Orai3 channels that were completely deprived of store-dependent activation. Lis *et al.* (31) have recently reported that an Orai3 K60E mutant similarly fails to be activated upon store depletion. Nevertheless, both the Orai3 ΔN_{1-57} and Orai3 K60E (31) mutants were still able to couple to STIM1 233–474 and CAD, respectively, used as surrogates of STIM1. Co-localization and density profiles of Orai3 ΔN_{1-57} and STIM1 233–474 indicated a reduced overall affinity compared with the fully functional Orai3 ΔN_{1-53}. This weaker binding apparently reflected the contribution of the N terminus for STIM1 binding despite the predominant role of the Orai C terminus in mediating STIM1/Orai coupling (10, 24). This finding is in accordance with the co-immunoprecipitation studies of Lis *et al.* (31) that showed retained but weaker binding of CAD to an N-terminal peptide mimicking Orai3 K60E *versus* Orai3. Thus, the N-terminal region downstream of aa 55 and particularly of Lys^{60} (31) plays a key role in transducing the coupling with STIM1 into Orai3 gating and current activation.

Although N-terminal truncation until aa 57 completely abolished store-operated activation, shorter truncations up to residue 51 maintained STIM1-dependent activation similar to wild-type Orai3. However, truncations within the stretch of residues from 51 to 55 increased current activation and altered gating characteristics of Orai3 channels. This effect less likely resulted from enhanced STIM1 binding to respective truncation mutants (Fig. 5, *d* and *e*) but rather resulted from an alteration of Orai3 gating with the change from fast inactivation into a profound potentiation phase. Here, the two arginines within this N-terminal stretch substantially affected Orai3 gating.

The unique fast inactivation of Orai3 required the whole conserved region (aa 48–65) of the Orai3 N terminus together with Arg^{47}. This region functions as a CaM-binding domain in Orai1 fast inactivation (16). In Orai3, CaM plays a similar role in fast inactivation as the reduction of CaM binding with increasing truncations correlated well with diminished fast inactivation (see Fig. 3). Hence, significantly reduced inactivation of Orai3 $\Delta N_{1-47/49/51}$ most likely reflects a concomitant decrease of CaM binding affinity as demonstrated here by *in vitro* binding assays. Point mutations disrupting CaM binding in Orai1 (16) were analogously introduced in Orai3 (Orai3 A48E and Orai3 W51E). We observed a similar loss of inactivation in accordance with the impaired fast inactivation of $\Delta N_{1-47/49/51}$ (data not shown), further underlining the involvement of CaM in Orai3 fast inactivation. Loss of CaM binding accompanied abrogation of fast inactivation of Orai3 $\Delta N_{1-53/55}$. Here, we identified the two arginines 52/53 in the center of the conserved region as further determinants for CaM binding and inactivation. Their deletion or mutation to alanines completely eliminated both CaM binding and fast inactivation. In addition, the Orai3 $\Delta N_{1-53/55}$ and Orai3 ΔN_{1-51} R52A/R53A mutants exhibited a pronounced potentiation and an increase in maximum current levels that exhibited U-shaped I/V characteristics. These effects might reflect an additional gating process.

Recently, a CRAC regulator protein (CRACR2A/B) has been identified to facilitate and stabilize STIM1-Orai complex formation (34). Its proposed interaction site on the Orai N terminus overlaps with that of CaM and can be disrupted in Orai1 by a double point mutation, K85A/K87A (34). To determine whether this protein is additionally involved in the regulation of Orai3 via its N terminus, we carried out knockdown as well as overexpression studies. Utilizing siRNA, suppression of endogenous CRACR2A but not of CRACR2B in HEK cells significantly inhibited STIM1/Orai1 current activation (supplemental Fig. 6a). However, neither STIM1/Orai3 currents nor their inactivation was affected by knockdown or overexpression of CRACR2A or CRACR2B (supplemental Fig. 6, b–e). Under the above conditions, Orai3 ΔN_{1-53} current characteristics were also not altered (supplemental Fig. 6, f–i). Hence, an involvement of CRACR2A/2B in regard to the changes of gating characteristics of wild type and Orai3 truncated forms is very unlikely.

We demonstrated that Orai3 channels required a minimal N-terminal segment starting from aa 56/57 to retain STIM1-dependent activation as well as 2-APB stimulation. 2-APB-stimulated outward currents were activated with some delay compared with inward currents (data not shown) as reported previously (35). Upon further deletion of aa 57, Orai3 lost store-operated current activation. Stimulation by 2-APB was maintained although to a reduced extent. Consistent with Orai3 ΔN_{1-57}, the Orai3 K60E mutant that fails to respond to store depletion similarly exhibits reduced 2-APB-stimulated currents (31). Furthermore, these reduced 2-APB currents displayed no delay in the activation of outward *versus* inward currents (data not shown). It might be hypothesized that the weaker binding of STIM1 to store-non-responsive N-terminal Orai3 truncation mutants might have allowed activation of inward and outward currents at a similar time course consistent with results of Yamashita *et al.* (35). As the truncation mutants that lost store-operated current activation concomitantly exhibited diminished 2-APB stimulation, we suggest that activations of Orai3 via STIM1 and 2-APB share some structural determinants. Moreover, the truncations might impose structural effects on the tetrameric channel, affecting distant conformational multidomain sites for 2-APB binding. We additionally observed for these 2-APB-responsive truncation mutants slightly right-shifted reversal potentials as compared with 2-APB-stimulated Orai3 wild-type currents. Thus, it is tempt-

ing to speculate that truncation of approximately two-thirds of the conserved N-terminal region might impose an allosteric effect upon the first transmembrane region, thereby altering channel pore conformation of the Orai3 ΔN_{1-57} (or shorter) mutants. In summary, we have pinpointed several key residues within the N-terminal conserved region of Orai3 that play an essential role in STIM1- as well as 2-APB-stimulated activation and current gating processes of Orai3.

Acknowledgments—We thank S. Buchegger for excellent technical assistance and Rainer Schindl for comments on the manuscript.

REFERENCES

1. Hoth, M., and Penner, R. (1992) *Nature* **355,** 353–356
2. Zweifach, A., and Lewis, R. S. (1993) *Proc. Natl. Acad. Sci. U.S.A.* **90,** 6295–6299
3. Parekh, A. B., and Putney, J. W., Jr. (2005) *Physiol. Rev.* **85,** 757–810
4. Prakriya, M., and Lewis, R. S. (2003) *Cell Calcium* **33,** 311–321
5. Roos, J., DiGregorio, P. J., Yeromin, A. V., Ohlsen, K., Lioudyno, M., Zhang, S., Safrina, O., Kozak, J. A., Wagner, S. L., Cahalan, M. D., Veliçelebi, G., and Stauderman, K. A. (2005) *J. Cell Biol.* **169,** 435–445
6. Luik, R. M., Wu, M. M., Buchanan, J., and Lewis, R. S. (2006) *J. Cell Biol.* **174,** 815–825
7. Liou, J., Kim, M. L., Heo, W. D., Jones, J. T., Myers, J. W., Ferrell, J. E., Jr., and Meyer, T. (2005) *Curr. Biol.* **15,** 1235–1241
8. Wu, M. M., Buchanan, J., Luik, R. M., and Lewis, R. S. (2006) *J. Cell Biol.* **174,** 803–813
9. Baba, Y., Hayashi, K., Fujii, Y., Mizushima, A., Watarai, H., Wakamori, M., Numaga, T., Mori, Y., Iino, M., Hikida, M., and Kurosaki, T. (2006) *Proc. Natl. Acad. Sci. U.S.A.* **103,** 16704–16709
10. Muik, M., Frischauf, I., Derler, I., Fahrner, M., Bergsmann, J., Eder, P., Schindl, R., Hesch, C., Polzinger, B., Fritsch, R., Kahr, H., Madl, J., Gruber, H., Groschner, K., and Romanin, C. (2008) *J. Biol. Chem.* **283,** 8014–8022
11. Lee, K. P., Yuan, J. P., Zeng, W., So, I., Worley, P. F., and Muallem, S. (2009) *Proc. Natl. Acad. Sci. U.S.A.* **106,** 14687–14692
12. Lis, A., Peinelt, C., Beck, A., Parvez, S., Monteilh-Zoller, M., Fleig, A., and Penner, R. (2007) *Curr. Biol.* **17,** 794–800
13. DeHaven, W. I., Smyth, J. T., Boyles, R. R., and Putney, J. W., Jr. (2007) *J. Biol. Chem.* **282,** 17548–17556
14. Frischauf, I., Schindl, R., Bergsmann, J., Derler, I., Fahrner, M., Muik, M., Fritsch, R., Lackner, B., Groschner, K., and Romanin, C. (2011) *J. Biol. Chem.* **286,** 8577–8584
15. Srikanth, S., Jung, H. J., Ribalet, B., and Gwack, Y. (2010) *J. Biol. Chem.* **285,** 5066–5075
16. Mullins, F. M., Park, C. Y., Dolmetsch, R. E., and Lewis, R. S. (2009) *Proc. Natl. Acad. Sci. U.S.A.* **106,** 15495–15500
17. Litjens, T., Harland, M. L., Roberts, M. L., Barritt, G. J., and Rychkov, G. Y. (2004) *J. Physiol.* **558,** 85–97
18. Yamashita, M., Navarro-Borelly, L., McNally, B. A., and Prakriya, M. (2007) *J. Gen. Physiol.* **130,** 525–540
19. Derler, I., Fahrner, M., Carugo, O., Muik, M., Bergsmann, J., Schindl, R., Frischauf, I., Eshaghi, S., and Romanin, C. (2009) *J. Biol. Chem.* **284,** 15903–15915
20. Peinelt, C., Lis, A., Beck, A., Fleig, A., and Penner, R. (2008) *J. Physiol.* **586,** 3061–3073
21. DeHaven, W. I., Smyth, J. T., Boyles, R. R., Bird, G. S., and Putney, J. W., Jr. (2008) *J. Biol. Chem.* **283,** 19265–19273
22. Schindl, R., Bergsmann, J., Frischauf, I., Derler, I., Fahrner, M., Muik, M., Fritsch, R., Groschner, K., and Romanin, C. (2008) *J. Biol. Chem.* **283,** 20261–20267
23. Zhang, S. L., Kozak, J. A., Jiang, W., Yeromin, A. V., Chen, J., Yu, Y., Penna, A., Shen, W., Chi, V., and Cahalan, M. D. (2008) *J. Biol. Chem.* **283,** 17662–17671
24. Frischauf, I., Muik, M., Derler, I., Bergsmann, J., Fahrner, M., Schindl, R., Groschner, K., and Romanin, C. (2009) *J. Biol. Chem.* **284,** 21696–21706
25. Korzeniowski, M. K., Manjarrés, I. M., Varnai, P., and Balla, T. (2010) *Sci. Signal.* **3,** ra82
26. Muik, M., Fahrner, M., Schindl, R., Stathopulos, P., Frischauf, I., Derler, I., Plenk, P., Lackner, B., Groschner, K., Ikura, M., and Romanin, C. (2011) *EMBO J.* **30,** 1678–1689
27. Li, Z., Lu, J., Xu, P., Xie, X., Chen, L., and Xu, T. (2007) *J. Biol. Chem.* **282,** 29448–29456
28. Yuan, J. P., Zeng, W., Dorwart, M. R., Choi, Y. J., Worley, P. F., and Muallem, S. (2009) *Nat. Cell Biol.* **11,** 337–343
29. Fahrner, M., Muik, M., Derler, I., Schindl, R., Fritsch, R., Frischauf, I., and Romanin, C. (2009) *Immunol. Rev.* **231,** 99–112
30. Park, C. Y., Hoover, P. J., Mullins, F. M., Bachhawat, P., Covington, E. D., Raunser, S., Walz, T., Garcia, K. C., Dolmetsch, R. E., and Lewis, R. S. (2009) *Cell* **136,** 876–890
31. Lis, A., Zierler, S., Peinelt, C., Fleig, A., and Penner, R. (2010) *J. Gen. Physiol.* **136,** 673–686
32. Singh, A., Hamedinger, D., Hoda, J. C., Gebhart, M., Koschak, A., Romanin, C., and Striessnig, J. (2006) *Nat. Neurosci.* **9,** 1108–1116
33. Muik, M., Fahrner, M., Derler, I., Schindl, R., Bergsmann, J., Frischauf, I., Groschner, K., and Romanin, C. (2009) *J. Biol. Chem.* **284,** 8421–8426
34. Srikanth, S., Jung, H. J., Kim, K. D., Souda, P., Whitelegge, J., and Gwack, Y. (2010) *Nat. Cell Biol.* **12,** 436–446
35. Yamashita, M., Somasundaram, A., and Prakriya, M. (2011) *J. Biol. Chem.* **286,** 9429–9442